

# The Lick-Carnegie Survey: A New Two-Planet System Around the Star HD 207832

Nader Haghighipour<sup>1</sup>, R. Paul Butler<sup>2</sup>, Eugenio J. Rivera<sup>3</sup>, Gregory W. Henry<sup>4</sup>, and Steven S. Vogt<sup>3</sup>,

## ABSTRACT

Keck/HIRES precision radial velocities of HD 207832 indicate the presence of two Jovian-type planetary companions in Keplerian orbits around this G star. The planets have minimum masses of  $M \sin i = 0.56 M_{\text{Jup}}$  and  $0.73 M_{\text{Jup}}$ , with orbital periods of  $\sim 162$  and  $\sim 1156$  days, and eccentricities of 0.13 and 0.27, respectively. Strömgren  $b$  and  $y$  photometry reveals a clear stellar rotation signature of the host star with a period of 17.8 days, well separated from the period of the radial velocity variations, reinforcing their Keplerian origin. The values of the semimajor axes of the planets suggest that these objects have migrated from the region of giant planet formation to closer orbits. In order to examine the possibility of the existence of additional (small) planets in the system, we studied the orbital stability of hypothetical terrestrial-sized objects in the region between the two planets and interior to the orbit of the inner body. Results indicated that stable orbits exist only in a small region interior to planet b. However, the current observational data offer no evidence for the existence of additional objects in this system.

*Subject headings:* stars: individual: HD 207832 – stars: planetary systems

---

<sup>1</sup>Institute for Astronomy and NASA Astrobiology Institute, University of Hawaii-Manoa, Honolulu, HI 96822

<sup>2</sup>Department of Terrestrial Magnetism, Carnegie Institute of Washington, Washington, DC 20015

<sup>3</sup>UCO/Lick Observatory, Department of Astronomy and Astrophysics, University of California at Santa Cruz, Santa Cruz, CA 95064

<sup>4</sup>Center of Excellence in Information Systems, Tennessee State University, Nashville, TN 37209

## 1. Introduction

The planetary census has currently exceeded an impressive 750 extrasolar planets. Planetary companions have been successfully detected using a variety of techniques, primarily radial velocity and transit photometry, with more than 700 and close to 230 planets detected by each method, respectively. Other successful techniques include microlensing (15 planets, see e.g., Batista et al. 2011), astrometry (e.g., Muterspaugh et al. 2010), stellar pulsations (Silvotti et al. 2007), direct imaging (31 planets, see e.g., Chauvin et al. 2005; Kalas et al. 2008; Marois et al., 2010), and the transit timing variation method (16 planets, see e.g., Holman et al. 2010; Lissauer et al. 2011; Doyle et al. 2011; Welsh et al. 2012).

The radial velocity method has been used to characterize  $\sim 92\%$  of all known planets, and continues to be the dominant technique. Both its continued productivity and its ability to accurately probe planetary architectures into the vicinity of the terrestrial-mass region (e.g., Rivera et al. 2005; Mayor et al. 2009; Vogt et al. 2010; Anglada-Escudé et al. 2012) are a testament to the capability of this technique and its rapid technological advances. For the past 18 years, we have used this technique and monitored a large number of nearby stars with the High Resolution Echelle Spectrometer (HIRES) at the Keck observatory. In this paper, we present new radial velocity (RV) and photometric observations for one of our target stars: HD 207832.

The plan of this paper is as follows. In §2, we discuss the basic properties of HD 207832. In §3, we describe the new radial velocities, derive a Keplerian two-planet model of the system, and describe the new APT observations. Finally, in §4, we discuss the properties of this new planetary system and the possibility of its hosting other planetary bodies.

## 2. HD 207832 Properties

HD 207832 (also known as CD-2615858, CPD-267292, SAO190699, 2MASSJ21523626-2601352, HIP 107985, and TYC6956-00378-1) is a G5 dwarf with a visual magnitude of  $8.786 \pm 0.014$ . We present in Table 1 a few basic parameters of this star. Unless otherwise noted, the data are as listed in the SPOCS (Valenti & Fischer 2005) and the NASA NStED databases<sup>5</sup>.

HD 207832 has a metallicity of  $[Fe/H]=0.06$  and an age  $< 4.5$  Gyr (Holmberg et al 2009). The parallax of this star, as revised by van Leeuwen (2007), is  $18.37 \pm 0.92$  mas,

---

<sup>5</sup><http://nsted.ipac.caltech.edu/>

which corresponds to a distance of  $54.4 \pm 2.7$  pc. As a result, HD 207832 has an absolute visual magnitude ( $M_v$ ) of  $5.11 \pm 0.11$ . The bolometric correction of HD 207832 in the visual is  $-0.080 \pm 0.055$  (Masana, Jordi, & Ribas 2006) implying an absolute bolometric magnitude of  $5.03 \pm 0.12$ . Assuming 4.75 for the corresponding quantity for the Sun, this bolometric magnitude points to a luminosity of  $0.773 \pm 0.085 L_\odot$  for this G star.

The simple mass-luminosity relationship for main sequence stars,  $M = L^{1/3.9}$ , indicates that the mass of HD 207832 is approximately  $0.94 \pm 0.10 M_\odot$ . This is in good agreement with the value determined from interpolation tables in Gray (1992) and the value of  $0.97 M_\odot$  as reported by Nordstroem et al. (2004). HD 207832 has a semi-diameter of  $0.077 \pm 0.001$  mas (Masana et al. 2006), which given its distance of 54.4 pc, indicates a stellar radius of  $0.901 \pm 0.056 R_\odot$ . Using the above-mentioned values of mass and radius, we find a simplistic estimate for  $\log g = 4.502 \pm 0.071$ , in good agreement with the expected range of values for a main sequence G star. The effective temperature of HD 207832, obtained from the Stefan-Boltzmann law with the luminosity and radius as mentioned above, is  $5710 \pm 81$  K, which is in rough agreement with 5649 K as reported by Holmberg et al. (2009).

The value of  $V \sin i$  for HD 207832 is approximately  $3 \text{ km s}^{-1}$  (Nordstroem et al. 2004). From our photometry presented in the next section, we determined a rotation period of 17.8 days. While obtaining the RV's presented here, we measured the Mt. Wilson  $S$  index and found that it has a mean value of 0.258. We also measured  $\log R'_{\text{HK}} = -4.62$ . These values are similar to  $S = 0.207$  and  $\log R'_{\text{HK}} = -4.80$ , as in Jenkins et al. (2008).

### 3. New Radial Velocity and Photometric Observations

#### 3.1. Radial Velocities

The HIRES spectrometer (Vogt et al. 1994) of the Keck-I telescope was used for all the new RV's presented in this paper. Doppler shifts were measured in the usual manner (Butler et al. 2006) by placing a gaseous Iodine absorption cell just ahead of the spectrometer slit in the converging beam from the telescope. This Iodine cell superimposes a rich forest of Iodine lines on the stellar spectrum, providing a wavelength calibration and proxy for the point spread function (PSF) of the spectrometer. The Iodine cell is sealed and temperature-controlled to  $50 \pm 0.1$  C such that the column density of Iodine remains constant. For the Keck planet search program, we operate the HIRES spectrometer at a spectral resolving power  $R \approx 70,000$  and wavelength range of 3700-8000 Å, though only the region 5000-6200 Å (with Iodine lines) is used in the present Doppler analysis. The Iodine region is divided into  $\sim 700$  wavelength intervals of 2 Å each. Each interval produces an independent measure of

the wavelength, PSF, and Doppler shift. The final measured velocity is the weighted mean of the velocities of the individual intervals. All radial velocities have been corrected to the solar system barycenter, but are not tied to any absolute radial velocity system. As such, they are “relative” radial velocities.

Table 2 lists the complete set of 86 relative RV’s for HD 207832, corrected to the solar system barycenter. We present results using only the internal uncertainties. The median internal uncertainty for our observations is  $1.95 \text{ m s}^{-1}$ , the peak-to-peak velocity variation is  $95.84 \text{ m s}^{-1}$ , and the velocity scatter around the mean RV is  $21.29 \text{ m s}^{-1}$ . The internal uncertainties quoted for all the RV’s in this paper reflect only one term in the overall error budget and result from a host of systematic errors such as characterizing and determining the PSF, detector imperfections, optical aberrations, effects of under-sampling the Iodine lines, etc. Two additional major sources of error are photon statistics and stellar jitter. The latter, which varies substantially from star to star, can be mitigated to some degree by selecting magnetically-inactive older stars and by time-averaging over the star’s unresolved low-degree surface p-modes. For HD 207832, the expected jitter is  $4.22 \text{ m s}^{-1}$  (Isaacson & Fischer 2010). This is in accord with the modest level of activity suggested by the quoted values of  $\log R'_{\text{HK}}$ . All observations have been further binned on 2-hour timescales.

Figure 1 shows the results. The top panel of this figure shows the individual RV observations, and the middle panel shows the weighted Lomb-Scargle (LS) periodogram of the full RV data set (Gilliland & Baliunas 1987). In generating this periodogram, we used only the internal uncertainties in the statistical weights and did not include jitter. To examine the effect of jitter, we added in quadrature  $4.22 \text{ m s}^{-1}$  to each internal uncertainty and reproduced the periodogram. The results showed only negligible differences.

The three horizontal lines in this figure and other comparable plots represent, from top to bottom, the 0.1%, 1.0%, and 10.0% False Alarm Probability (FAP) levels, respectively. The algorithm for computing the LS periodogram is described in detail in §13.8 of Press et al. (1992). To estimate our FAP levels, we randomly assign (without replacement) an observed RV – or residual RV when we consider the residuals for a fit – (with its corresponding uncertainty) to each observing epoch. We repeat this  $10^5$  times. For each synthetic RV (or residual RV) set generated in this manner, we compute the weighted LS periodogram. Our FAP estimates are then the fraction of these periodograms in which the power in the tallest peak equals or exceeds the power in the periodogram of the real RVs (or residual RVs). We do this to circumvent potential problems associated with the application of the FAP estimation method(s) in Press et al. (1992), which are strictly applicable only in the case of single, isolated signals in the presence of Gaussian noise with known variance (Koen 1990). For the strong Keplerian signal at  $P \sim 162$  days in the RV data set, we find a FAP

$< 10^{-5}$ . Finally, the lower panel of Figure 1 shows the power spectral window. This spectral window indicates spurious power that might be introduced into the data from the choice of sampling times alone, and it can be used to aid in the identification of aliased signals.

### 3.2. Keplerian Solution

Table 3 summarizes a one-planet Keplerian fit for HD 207832. Orbital fits were derived using the Systemic Console (Meschiari et al. 2009)<sup>6</sup>. The errors on each parameter are estimated using the bootstrap technique with 1000 realizations of the RV data sets. We fit all the realizations, and the uncertainties in the best-fit parameters are determined by the ranges in each parameter containing 68.2% of the distributions of the fitted values. For each planet, we list best-fit period ( $P$ ), eccentricity ( $e$ ), semi-amplitude ( $K$ ), longitude of pericenter ( $\varpi$ ), mean-anomaly (MA), minimum mass ( $M \sin i$ ) and semi-major axis ( $a$ ).

The dominant peak in the periodogram of the RV’s is well fitted with a Keplerian orbit of period 161.82 days and semi-amplitude  $K = 21.30 \text{ m s}^{-1}$  (top panel of Figure 2). Together with the assumed stellar mass of  $0.94 M_{\odot}$ , this amplitude suggests a planet with a minimum mass of  $M \sin i = 0.62 M_{\text{Jup}}$ . The best-fit orbit for this planet is moderately eccentric ( $e \approx 0.18$ ). This one-planet fit achieves  $\chi_{\nu}^2 = 43.99$ , with an RMS of  $12.33 \text{ m s}^{-1}$ . If we add in the estimated jitter and perform a new fit, the only significant difference will be the reduction of  $\chi_{\nu}^2$  to 8.22. Within the uncertainties, the two fits were indistinguishable.

The bottom panel of Figure 2 shows the periodogram of the residuals to the single-planet fit. The dominant peak at  $P = 1111.2$  days with a FAP  $2.3 \times 10^{-4}$  is indicative of a secure detection of an additional planet. Again, we find that the addition of the expected jitter to the internal uncertainties has a minor effect on this periodogram. The peak near 30 days is an alias of the 1111-day peak. In fact, the 30, 150, and 1111-day peaks in the one-planet residuals periodogram are all inter-related via the lunar synodic and 1/2-year peak in the Power Spectral Window of Figure 1 (bottom panel).

Our best combined two-planet fit indicates a second planet with  $P = 1155.70$  days,  $K = 15.34 \text{ m s}^{-1}$ , and a minimum mass of  $M \sin i = 0.73 M_{\text{Jup}}$  (Table 4). The best-fit orbital model of the second planet suggests a moderate eccentricity, ( $e \approx 0.27$ ). With this revised fit, we obtain  $\chi_{\nu}^2 = 22.93$  and an RMS of the residuals of  $8.43 \text{ m s}^{-1}$ . The F-test of the two-planet fit vs. the one-planet fit gives a probability of  $5 \times 10^{-4}$  (based on the

---

<sup>6</sup>Downloadable at <http://www.oklo.org>

difference in RMS values<sup>7</sup>) that the two-planet fit is not significantly different from the one-planet fit, indicating further evidence in support of the two planet model. Similar to the case of the one-planet fit, the only significant result of adding in the expected jitter is that for this two-planet model,  $\chi_\nu^2$  will be reduced to 4.05. As with the one-planet model, within the uncertainties, the fitted parameters for fits with and without jitter have negligible differences.

Figure 3 shows phase folded RV’s for the two-planet fit. The top panel corresponds to the case where the period of the inner planet has been used and the effect of the outer planet has been subtracted. Similarly, the middle panel is for the case where the period of the outer planet was used and the effect of the inner planet was subtracted. The bottom panel of this figure shows the periodogram of the residuals of the best-fit solution. The FAP of the tallest peak is  $\sim 50\%$ . The corresponding result when we added in the expected jitter was similar, although the period of the tallest peak was slightly different. The current data set thus offers no compelling evidence for additional planets.<sup>8</sup>

The periodograms of the residuals of the two-planet fits (with and without the addition of the expected jitter) contain peaks (of little significance) with periods ranging from 18 to 22 days. Also, the analysis of the Mt. Wilson  $S$  index indicates a periodicity of  $\sim 19$  days. These values are in rough agreement with the photometric period discussed in the next section. Inspection of the individual seasons of the  $S$ , RV, and photometric observations indicates that there is significant variation in the peak period (and its associated power) in the periodograms of these quantities. These weak periodicities may be tied to the rotation period of the star through the presence of stellar spots and chromospheric activity. The lack of a strong coherent signal over the full time spans of the observations and the relatively large power levels in the periodogram of the two-planet residuals suggest the presence of additional (non-Gaussian) noise. Since the FAP for the most prominent signals in the residuals of the two-planet fit are  $\sim 50\%$  and there is evidence for additional noise which does not show strong coherence over the time span of the observations, we do not attempt to fit for the stellar rotation (and any other potential remaining signals).

---

<sup>7</sup>This value reduces drastically to  $3 \times 10^{-10}$  when calculated based on the difference in  $\chi_\nu^2$ .

<sup>8</sup>As a check of the reliability of our results, we calculated FAPs for our one- and two-planet fits as well as for the most prominent signal in the residuals, using the formalism presented by Baluev (2008). In agreement with our previous calculations, we found that for the one-planet fit,  $\text{FAP} < 10^{-16}$ , for the two-planet fit, it is  $< 10^{-5}$ , and for the residuals, it is  $< 0.5$ . The periodograms for each case were equivalent to those shown in Figures 1-3, confirming the secure detection of the two planets.

### 3.3. APT Photometry

In addition to the Keck radial velocities, we obtained Strömbergren  $b$  and  $y$  photometric observations with the T12 0.80 m automatic photometric telescope (APT) at Fairborn Observatory in Arizona. The T12 APT uses a two-channel precision photometer with two EMI 9124QB bi-alkali photomultiplier tubes to make simultaneous measurements in the two passbands. We programmed the APT to make differential brightness measurements of HD 207832 ( $V = 8.78$ ,  $B - V = 0.69$ , G5 V) with respect to three comparison stars: HD 207760 ( $V = 6.19$ ,  $B - V = 0.37$ , F0 V), HD 206797 ( $V = 7.35$ ,  $B - V = 0.40$ , F2 III), and HD 208483 ( $V = 7.64$ ,  $B - V = 0.48$ , F4 V). A detailed description of the automatic telescope, precision photometer, observing procedures, data reduction, calibration, and photometric precision can be found in Henry (1999). The typical precision of a single observation is approximately 0.0015 mag on good nights.

The T12 APT acquired 310 differential observations of HD 207832 during the 2007 – 2010 observing seasons. The observing seasons are short, two or three months, because the star’s declination is  $-26^\circ$ , making it difficult to observe from Arizona. Also, the star comes to opposition in mid-August when the Fairborn APT site is forced to shut down for two months by the annual monsoons. To improve the photometric precision of these relatively high-airmass observations, we combined our differential  $b$  and  $y$  observations into a single  $(b + y)/2$  passband. We also computed all differential magnitudes using the composite mean brightness of the three comparison stars to average out any subtle light variations in the comparisons.

The resulting differential magnitudes are plotted in the top panel of Figure 4 and are summarized in Table 5. Even though the observing seasons are short, it is clear from both the table and figure that the mean brightness of HD 207832 varies over a range of  $\sim 0.005$  mag. In contrast, the composite mean of the three comparison stars varies over a total range of only 0.0010 mag and has a standard deviation from the grand mean of only 0.00051 mag. This demonstrates the long-term stability of our photometric calibrations and the reliability of the measured variation in the yearly-mean brightness of HD 207832. The low-level photometric variability in HD 207832 results from subtle changes in the star’s magnetic activity and is in line with other solar-type stars of similar age (see, e.g., Figure 11 of Hall et al. 2009).

The presence of photospheric spots in solar-type stars allows the possibility of direct determination of stellar rotation periods due to rotational modulation in the visibility of the spots and the consequent variability in the star’s brightness (see, e.g., Gaidos et al. 2000; Henry et al. 1995). Queloz et al. (2001) and Paulson et al. (2004) have demonstrated how starspots can result in periodic radial velocity variations that mimic the presence of planetary companions. We performed periodogram analyses of the individual four seasons

of our HD 207832 photometry. Coherent brightness variability with a strong rotation signal was found only in the first observing season, plotted in the second panel of Figure 4. We note from column 4 of Table 5 that the 2007 season exhibited the largest night-to-night brightness variability, indicating a slightly larger degree of asymmetry in the spot distribution and so permitted the determination of the star’s rotation period. The frequency spectrum of these observations in the third panel of Figure 4 gives a period of  $17.8 \pm 0.5$  days. Much weaker signals of 20, 21, and 24 days were seen in 2008 and 2009 seasons, so we take 17.8 days to be the rotation period of HD 207832. This period is consistent with the star’s  $V \sin i = 3 \text{ km s}^{-1}$  and  $\log R'_{\text{HK}} = -4.62$ . The 2007 season data are phased with the rotation period in the bottom panel of Figure 4. The best-fit sine curve, also plotted in the bottom panel, has a peak-to-peak amplitude of 0.011 mag.

#### 4. Concluding Remarks

The measurements of the radial velocities of HD 207832 suggest that two Jovian-type planets exist in orbit around this star. Given the moderate eccentricities of these two planets and the small semi-major axis of the inner body, it would be interesting to speculate on the origin of these objects and the possibility of the existence of additional smaller bodies in this system.

As HD 207832 is a solar-type star with a mass only slightly smaller than that of the Sun, conventional wisdom holds that any Jovian-type planets associated with this star should have formed at large distances, beyond the protoplanetary “ice line”. This picture suggests that planet b and (possibly) planet c were formed in regions well separated from their current orbits and reached their current locations either via migration, interaction with other planetary bodies, or a combination of both.

Given that HD 207832 is a Sun-like star, it would not be unrealistic to assume that in the past, this star was surrounded by a disk of planetesimals and planetary embryos. The migration of the two planets of this system (in particular planet b) could have affected the dynamics of these protoplanetary bodies, scattering them out of the system and altering their accretion to larger (e.g., terrestrial-class) objects. Within the confines of this paradigm, it would be moderately unexpected to find a small planet orbiting in the region between planets b and c. Such an object, however, may be able to maintain stability in the region interior to planet b. As argued by Zhou et al. (2005), Fogg & Nelson (2005, 2006, 2007a,b, 2009), Raymond et al. (2008), and many other researchers, small planets might in fact form and survive inside the orbit of a migrating giant body.



To examine the possibility of the existence of terrestrial-class objects in the region between the two planets and interior to the orbit of planet b, we considered each planet to have an influence zone extending from  $a(1 - e) - 3R_H$  to  $a(1 + e) + 3R_H$ , where  $R_H$  is the planet’s Hill radius. An additional object will be outside these influence zones if its orbit is larger than 3 AU, between 0.75 and 1.25 AU, or smaller than 0.4 AU. We placed a hypothetical Earth-mass planet at different distances in the two regions nearer to the star and integrated the four-body system of the star, planets b and c, and the Earth-mass body for 1 Myr and for different values of the hypothetical planet’s semimajor axis. We assumed that the Earth-mass planet was initially in a circular orbit and varied its initial semimajor axis between 0.75 AU and 1.25 AU, and between 0.05 and 0.4 AU in increments of 0.01 AU. Results indicated that, between the two planets, in the region 0.75-1.25 AU, the orbits of all hypothetical bodies became unstable in less than 1 Myr. The orbits of the objects between 0.3 and 0.4 AU also became unstable in a few hundred thousand years. However, objects between 0.05 and 0.3 AU maintained their orbits for the duration of the integration.

Although these results indicate that a low-mass planet may be stable in a small region interior to the orbit of HD 207832 b, it is not possible, based on the current observational data, to make a definite conclusion on the actual existence of this object. As mentioned before, the periodogram of the residuals of our best-fit model shows no significant signal, implying that the current observational data offer no significant evidence for other planets in this system.

NH acknowledges support from the NASA Astrobiology Institute under Cooperative Agreement NNA09DA77 at the Institute for Astronomy, University of Hawaii, and NASA EXOB grant NNX09AN05G. RPB acknowledges support from NASA OSS Grant NNX07AR40G, the NASA Keck PI program, and from the Carnegie Institution of Washington. GL acknowledges support from the NASA Astrobiology Institute at NASA Ames Research Center. GWH acknowledges support from NASA, NSF, Tennessee State University, and the State of Tennessee through its Centers of Excellence program. SSV gratefully acknowledges support from NSF grant AST-0307493. The work herein is based on observations obtained at the W. M. Keck Observatory, which is operated jointly by the University of California and the California Institute of Technology. We thank the UC-Keck, NASA-Keck, and UH/IFA Time Assignment Committees for their support. This research has made use of the SIMBAD database, operated at CDS, Strasbourg, France.

*Facilities:* Keck (HIRES).

## REFERENCES

- Anglada-Escudé, G., et al. 2012, *ApJL*, 751, article id. L16
- Baluev, R. V. 2008, *MNRAS*, 385, 1279
- Batista, V., et al. 2011, *A&A*, 529, id.A102
- Butler, R. P., Wright, J. T., Marcy, G. W., Fischer, D.A., Vogt, S. S., Tinney, C. G., Jones, H. R. A., Carter, B. D., Johnson, J. A., McCarthy, C., & Penny, A. J. 2006, *ApJ*, 646, 505
- Chauvin, G., Lagrange, A.-M., Zuckerman, B., Dumas, C., Mouillet, D., Song, I., Beuzit, J.-L., Lowrance, P., & Bessell, M. S. 2005, *A&A*, 438, L29
- Doyle, L. R., et al. 2011, *Science*, 333, 1602
- Gaidos, E. J., Henry, G. W., & Henry, S. M. 2000, *AJ*, 120, 1006
- Fogg, M. J., & Nelson, R. P. 2005, *A&A*, 441, 791
- Fogg, M. J., & Nelson, R. P. 2006, *Inter. J. Astrobio.*, 5, 199
- Fogg, M. J., & Nelson, R. P. 2007a, *A&A*, 461, 1195
- Fogg, M. J., & Nelson, R. P. 2007b, *A&A*, 472, 1003
- Fogg, M. J., & Nelson, R. P. 2009, *A&A*, 498, 575
- Gilliland, R. L., & Baliunas, S. L. 1987, *ApJ*, 314, 766
- Gray, D. F. 1992, *Camb. Astrophys. Ser.*, Vol. 20
- Hall, J. C., Henry, G. W., Lockwood, G. W., Skiff, B. A., & Saar, S. H. 2009, *AJ*, 138, 312
- Henry, G. W., Fekel, F. C., & Hall, D. S. 1995, *AJ*, 110, 2926
- Henry, G. W. 1999, *PASP*, 111, 845
- Holman, M. J., et al. 2010, *Science*, 330, 51
- Holmberg, J., Nordstroem, B., & Andersen, J. 2009, *A&A*, 501, 941
- Houk, N. 1982, *Michigan Catalog of Two-dimensional Spectral Types for the HD stars*, Ann Arbor, MI(USA): Department of Astronomy, University of Michigan

- Isaacson, H. & Fischer, D. 2010, *ApJ*, 725, 875
- Jenkins, J. S., Jones, H. R. A., Pavlenko, Y., Pinfield, D. J., Barnes J. R., & Lyubchik, Y. 2008, *A&A*, 485, 571
- Kalas, P., Graham, J. R., Chiang, E., Fitzgerald, M. P., Clampin, M., Kite, E. S., Stapelfeldt, K., Marois, C., & Krist, J. 2008, *Science*, 322, 1345
- Koen, C. 1990, *ApJ*, 348, 700
- Lissauer, J. J., et al. 2011, *Nature*, 470, 53
- Marois, C., Zuckerman, B., Konopacky, Q. M., Macintosh, B., & Barman, T. 2010, *Nature*, 468, 1080
- Masana, E., Jordi, C. & Ribas, I. 2006, *A&A*, 450, 735
- Muterspaugh, M. W., Lane, B. F., Kulkarni, S. R., Konacki, M., Burke, B. F., Colavita, M. M., Shao, M., Hartkopf, W. I., Boss, A. P., & Williamson, M. 2010, *ApJ*, 140, 1657
- Mayor, M., Bonfils, X., Forveille, T., Delfosse, X., Udry, S., Bertaux, J.-L., Beust, H., Bouchy, F., Lovis, C., Pepe, F., Perrier, C., Queloz, D., Santos, N. C. 2009, *A&A*, 507, 487
- Meschiari, S., Wolf, A. S., Rivera, E., Laughlin, G., Vogt, S., & Butler, P. 2009, *PASP*, 121, 1016
- Nordstroem, B., et al., 2004, *A&A*, 418, 989
- Paulson, D. B., Saar, S. H., Cochran, W. D., & Henry, G. W. 2004, *AJ*, 127, 1644
- Press, W. H., Teukolsky, S. A., Vetterling, W. T., & Flannery, B. P. 1992, *Numerical recipes in C. The art of scientific computing* (Cambridge: University Press, –c1992, 2nd ed.)
- Queloz et al. 2001, *A&A*, 379, 279
- Raymond, S. N., Barnes, R., & Mandell, A. M. 2008, *MNRAS*, 384, 663
- Rivera, E. J., Lissauer, J. J., Butler, R. P., Marcy, G. W., Vogt, S. S., Fischer, D. A., Brown, T. M., Laughlin, G., & Henry, G. W. 2005, *ApJ*, 634, 625
- Silvotti, R., et al. 2007, *Nature*, 449, 189
- Valenti, J. A., & Fischer, D. A. 2005, *ApJS*, 159, 141

van Leeuwen, F. 2007, *A&A*, 474, 653

Vogt, S. S., et al. 1994, in *Society of Photo-Optical Instrumentation Engineers (SPIE) Conference Series*, Vol. 2198, *Society of Photo-Optical Instrumentation Engineers (SPIE) Conference Series*, ed. D. L. Crawford & E. R. Craine, 362

Vogt, S. S., Butler, R. P., Rivera, E. J., Haghighipour, N., & Williamson, M. H. 2010, *ApJ*, 723, 954

Welsh, W. F., et al. 2012, *Nature*, 481, 475

Zhou, J.-L., Aarseth, S. J., Lin, D. N. C., and Nagasawa, M. 2005, *ApJ*, 631, L85

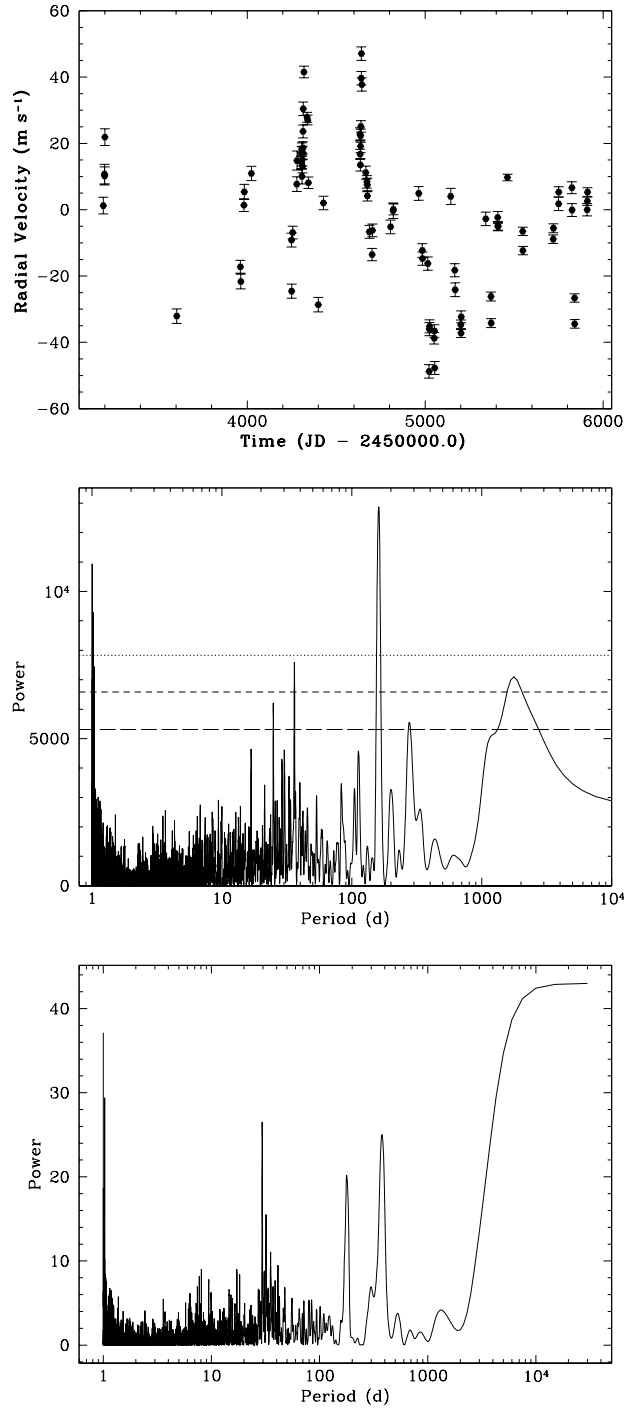


Fig. 1.— Radial velocity data and periodograms for HD 207832. *Top panel:* Relative HIRES/Keck radial velocity data. *Middle panel:* Weighted Lomb-Scargle periodogram of the radial velocity data. *Bottom panel:* Power spectral window.

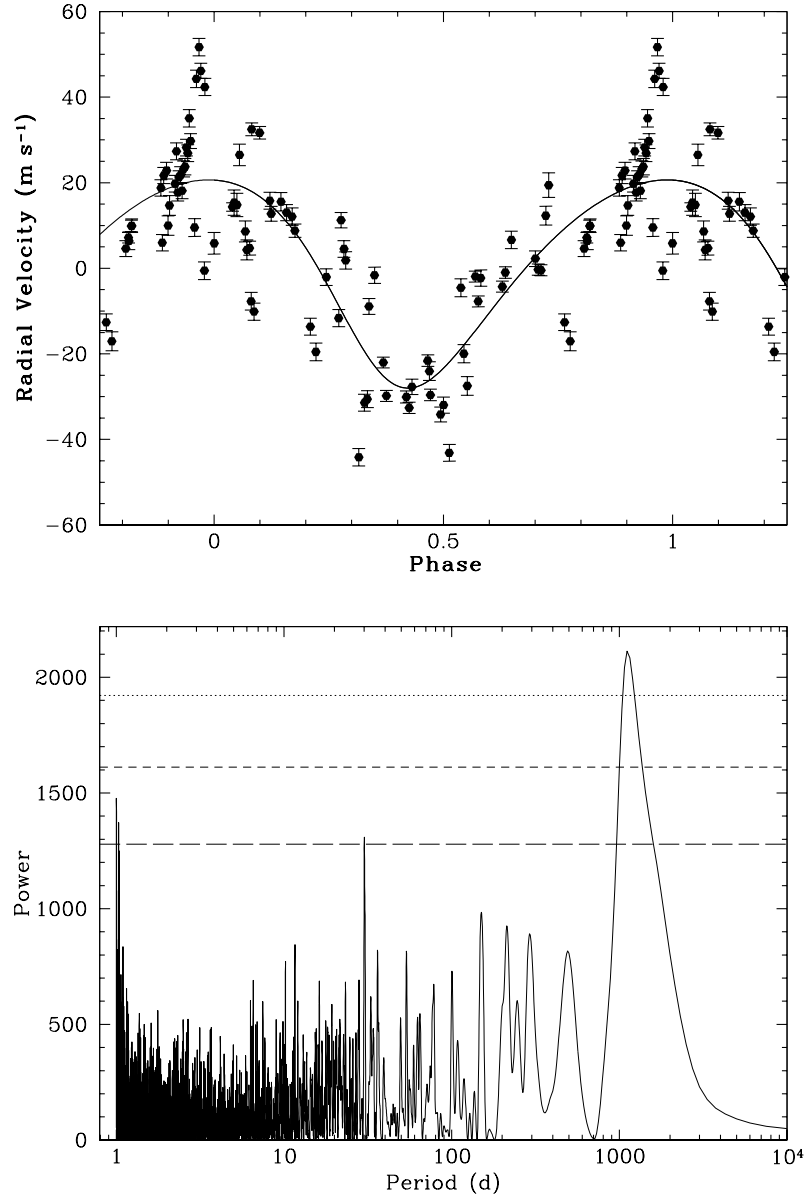


Fig. 2.— One-planet Keplerian solution and residuals periodogram for HD 207832. *Top panel:* Phased Keplerian fit. *Bottom panel:* Periodogram of the residuals to the one-planet best-fit solution.

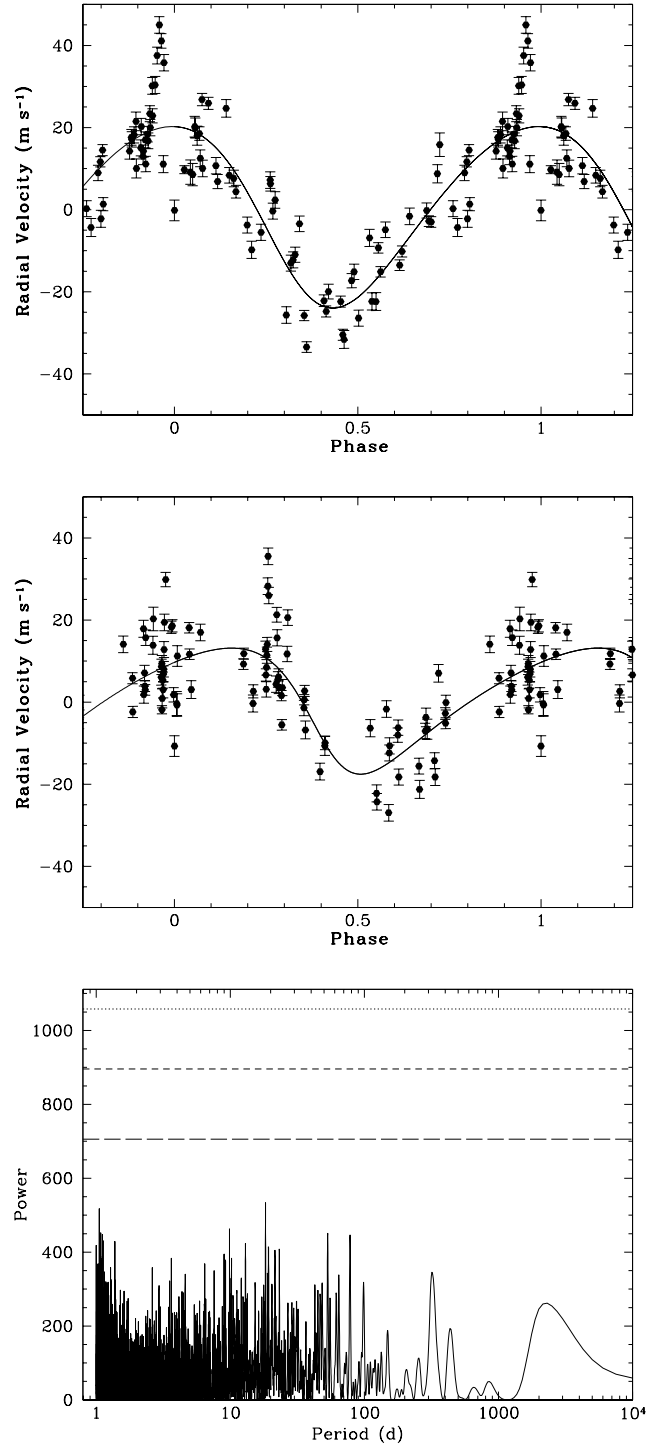


Fig. 3.— Keplerian solutions and residuals periodogram for HD 207832. *Top panel:* Phased Keplerian fit in a system where the period of the inner planet has been used and the effect of the outer planet has been subtracted. *Middle panel:* Phased Keplerian fit in a system where the period of the outer planet has been used and the effect of the inner planet has been subtracted. *Bottom panel:* Periodogram of the residuals to the two-planet best-fit solution.

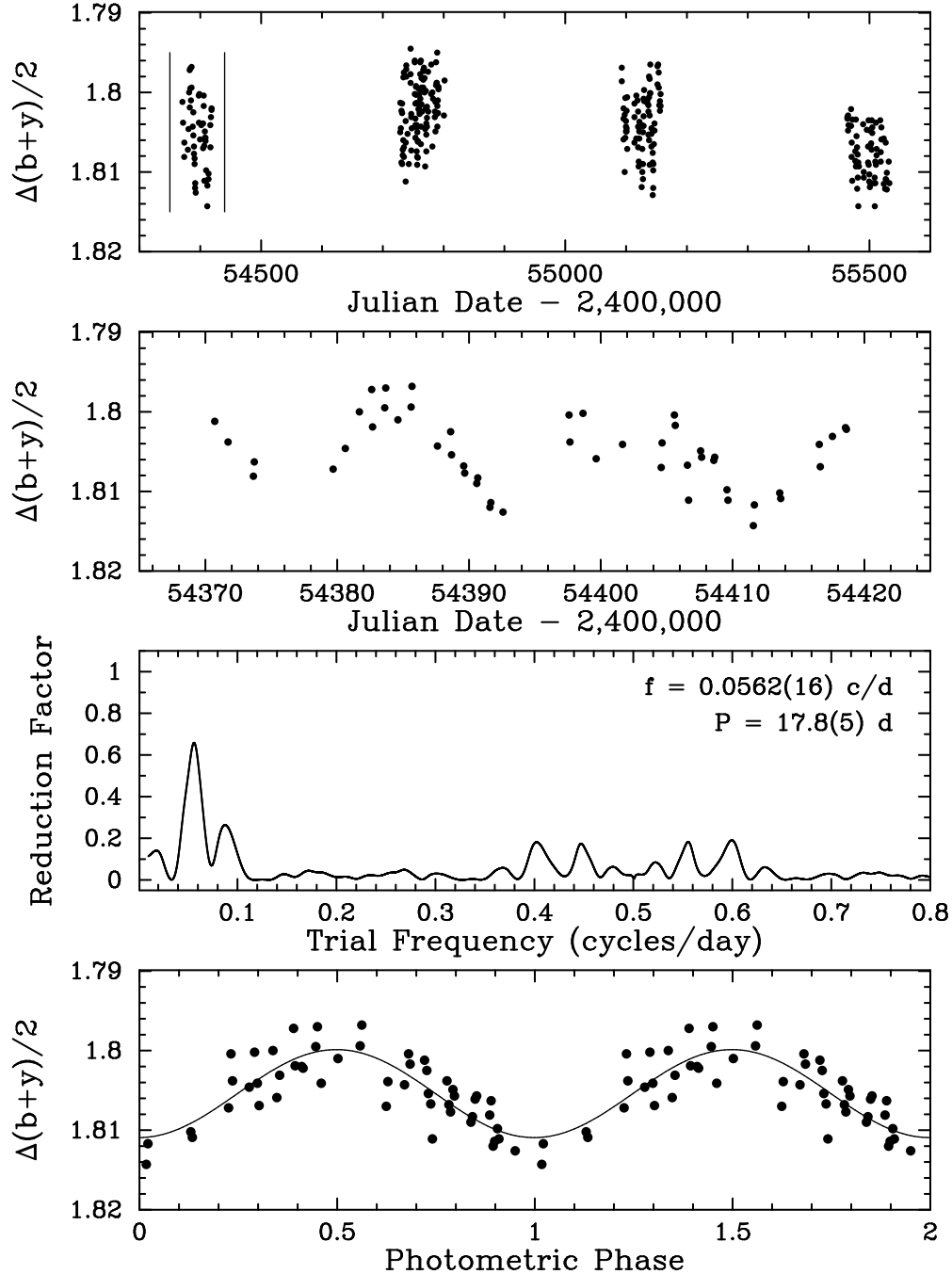


Fig. 4.— *Top*: The 310 photometric observations of HD 207832 in the  $(b + y)/2$  passband, acquired with the T12 0.8 m APT during the 2007, 2008, 2009, and 2010 observing seasons. *Second panel*: The 2007 observing season, set off with vertical bars in the top panel, showing the most coherent brightness variability due to cool starspots carried across the disk of the star by its rotation. *Third panel*: Frequency spectrum of the observations in the second panel giving a best period of  $17.8 \pm 0.5$  days. *Bottom Panel*: Plot of the data from panel two, phased with the star’s 17.8-day rotation period. Results reveal coherent variability with a peak-to-peak amplitude 0.011 mag.



Table 1. Stellar parameters for HD 207832

Parameter	Value	Reference
Spectral Type	G5V	Houk (1982)
$M_V$	$5.11 \pm 0.11$	Masana, Jordi, & Ribas (2006)
$B - V$	0.694	Hipparcos catalog
$V$	$8.786 \pm 0.014$	Hipparcos catalog
Mass ( $M_\odot$ )	$0.94 \pm 0.10$	This work
Radius ( $R_\odot$ )	$0.901 \pm 0.056$	This work
Luminosity ( $L_\odot$ )	$0.773 \pm 0.085$	This work
Distance (pc)	$54.4 \pm 2.7$	van Leeuwen (2007)
$V \sin i$ ( $\text{km s}^{-1}$ )	3.0	Nordstroem et al. (2004)
$S$	0.258	This work
$\log R'_{\text{HK}}$	-4.62	This work
Age (Gyr)	< 4.5	Holmberg et al (2009)
[Fe/H]	0.06	Holmberg et al (2009)
$T_{\text{eff}}$ (K)	$5710 \pm 81$	This work
$\log g$	$4.502 \pm 0.071$	This work
$P_{\text{rot}}$ (days)	17.8	This work
$M_{\text{bol},\odot}$	$5.03 \pm 0.12$	Masana, Jordi, & Ribas (2006)

Table 2. HIRES/Keck radial velocities for HD 207832

JD	RV ( $\text{m s}^{-1}$ )	Uncertainty ( $\text{m s}^{-1}$ )
2453191.07306	1.23	2.52
2453198.10964	10.76	2.96
2453199.10969	10.20	2.71
2453200.02832	21.89	2.50
2453604.05288	-32.09	2.18
2453962.02939	-17.22	1.94
2453964.03012	-21.66	2.20
2453981.83958	1.37	1.91
2453983.88414	5.39	2.27
2454023.73787	10.94	2.14
2454249.06943	-9.15	2.08
2454250.11123	-24.57	2.11
2454256.08362	-6.89	1.89
2454279.05384	7.69	2.21
2454280.07780	14.81	2.87
2454304.98079	14.17	1.91
2454305.97931	17.08	1.86
2454306.98351	18.22	1.95
2454308.00756	10.08	2.32
2454309.97308	15.16	1.96
2454310.96397	13.10	1.97
2454311.96209	17.20	1.95
2454312.95811	18.61	1.88
2454313.95461	23.62	1.95
2454314.98918	30.46	2.03
2454319.05290	41.53	1.76
2454336.99854	27.88	1.48
2454339.83047	27.06	1.48
2454343.90031	8.14	1.74
2454399.76550	-28.65	2.18
2454428.72442	2.04	2.02
2454634.11007	22.74	1.99
2454635.02452	16.73	1.48

Table 2—Continued

JD	RV ( $\text{m s}^{-1}$ )	Uncertainty ( $\text{m s}^{-1}$ )
2454636.07870	13.52	1.87
2454637.12316	19.12	1.91
2454638.07365	22.29	1.97
2454639.08741	25.12	1.72
2454641.11196	39.66	2.04
2454642.07952	47.08	2.03
2454644.10800	37.76	2.01
2454667.05175	11.18	1.99
2454672.98097	8.41	1.89
2454674.92028	7.48	2.03
2454675.92382	4.18	1.55
2454687.01449	-6.67	1.97
2454702.06135	-13.54	1.85
2454704.01682	-6.23	1.89
2454805.78129	-5.17	2.05
2454820.76637	-0.29	2.32
2454821.73081	0.11	1.64
2454964.12223	4.93	2.09
2454984.08389	-12.31	2.06
2454985.11255	-14.74	2.02
2455015.01571	-16.25	2.01
2455022.11297	-48.76	2.02
2455024.10459	-36.02	1.95
2455025.10763	-35.17	1.96
2455050.98600	-38.79	1.74
2455052.04273	-36.58	1.88
2455054.05711	-47.74	1.95
2455143.85599	4.02	2.44
2455166.79983	-18.24	1.96
2455168.76488	-24.14	2.09
2455200.70599	-34.68	1.42
2455201.70283	-37.22	1.33
2455202.70257	-32.32	1.79

Table 2—Continued

JD	RV ( $\text{m s}^{-1}$ )	Uncertainty ( $\text{m s}^{-1}$ )
2455341.10738	-2.76	2.01
2455370.09190	-26.18	1.34
2455371.02144	-34.21	1.35
2455408.08145	-2.35	1.83
2455409.05312	-4.91	1.29
2455410.05776	-5.07	1.30
2455462.94628	9.74	0.99
2455548.69542	-6.54	1.27
2455549.69363	-12.33	1.28
2455720.05565	-8.89	1.30
2455721.10910	-5.59	1.35
2455750.03262	1.80	2.06
2455751.03252	5.33	1.59
2455824.90900	6.65	1.79
2455825.96501	-0.09	1.96
2455839.83583	-26.64	1.25
2455840.91258	-34.41	1.29
2455910.72389	0.00	1.87
2455911.69779	2.56	1.24
2455912.71141	5.28	1.35

Table 3. Keplerian orbital solution for the one-planet fit

Parameter	HD 207832 b
$P$ (days)	$161.82^{+0.73}_{-1.69}$
$e$	$0.18^{+0.15}_{-0.07}$
$K$ ( $\text{m s}^{-1}$ )	$24.30^{+2.96}_{-0.94}$
$\varpi$ ( $^{\circ}$ )	$146.1^{+21.1}_{-115.1}$
MA ( $^{\circ}$ )	$231.2^{+78.4}_{-28.9}$
$M \sin i$ ( $M_{\text{Jup}}$ )	$0.62^{+0.06}_{-0.04}$
$a$ (AU)	$0.569^{+0.002}_{-0.005}$
Epoch (JD)	2453191.07306
$\chi^2_{\nu}$	43.99
RMS ( $\text{m s}^{-1}$ )	12.33

Table 4. Keplerian orbital solution for two-planet fit

Parameter	HD 207832 b	HD 207832 c
$P$ (days)	$161.97^{+0.97}_{-0.78}$	$1155.7^{+71.9}_{-37.0}$
$e$	$0.13^{+0.18}_{-0.05}$	$0.27^{+0.22}_{-0.10}$
$K$ ( $\text{m s}^{-1}$ )	$22.1^{+2.7}_{-1.3}$	$15.3^{+5.2}_{-1.0}$
$\varpi$ ( $^\circ$ )	$130.8^{+23.9}_{-83.4}$	$121.6^{+32.4}_{-76.5}$
MA ( $^\circ$ )	$243.3^{+83.2}_{-30.1}$	$211.9^{+114.4}_{-0.0}$
$M \sin i$ ( $M_{\text{Jup}}$ )	$0.56^{+0.06}_{-0.03}$	$0.73^{+0.18}_{-0.05}$
$a$ (AU)	$0.570^{+0.002}_{-0.002}$	$2.112^{+0.087}_{-0.045}$
Epoch (JD)	2453191.07306	
$\chi^2_\nu$	22.93	
RMS ( $\text{m s}^{-1}$ )	8.43	

Table 5. Summary of Photometric Observations for HD 207832

Observing Season (1)	$N_{\text{obs}}$ (2)	Date Range (HJD – 2,400,000) (3)	Sigma (mag) (4)	Seasonal Mean (mag) (5)
2007	50	54370–54418	0.00436	$1.80516 \pm 0.00062$
2008	111	54728–54801	0.00379	$1.80205 \pm 0.00036$
2009	82	55092–55156	0.00386	$1.80377 \pm 0.00043$
2010	67	55463–55532	0.00315	$1.80778 \pm 0.00038$